

Enhanced Phase Estimation via Photon-Added Two-Mode Squeezed States and Kerr Nonlinearity

Zekun Zhao¹, Qingqian Kang^{1,2}, Teng Zhao¹, Cunjin Liu¹, and Liyun Hu^{1,3*}

¹Center for Quantum Science and Technology, Jiangxi Normal University, Nanchang 330022, China

²Department of Physics, Jiangxi Normal University Science and Technology College, Nanchang 330022, China

³Institute for Military-Civilian Integration of Jiangxi Province, Nanchang 330200, China

Quantum metrology harnesses quantum resources to achieve measurement precision beyond classical limits. This work investigates a Mach-Zehnder interferometer incorporating a Kerr nonlinear phase shifter, using photon-added two-mode squeezed coherent states generated via four-wave mixing as input. This study demonstrates that increasing both the photon-addition order and input resource strength systematically enhances phase sensitivity, quantum Fisher information, and the quantum Cramér-Rao bound. The system not only surpasses the standard quantum limit but also approaches or exceeds the Heisenberg limit with linear phase shifts, while Kerr nonlinearity enables overcoming the super-Heisenberg limit. The proposed scheme exhibits enhanced robustness against photon loss, providing a promising approach for high-precision quantum metrology applications.

PACS: 03.67.-a, 05.30.-d, 42.50.Dv, 03.65.Wj

I. INTRODUCTION

Precision measurement constitutes the foundation of scientific and technological advancement, with its fundamental limits defining our capacity to understand and manipulate physical phenomena. From traditional mechanical manufacturing to modern lithography techniques, and from gravitational wave detection to biomedical sensing, technological progress consistently relies on advances in measurement precision. Within classical frameworks, however, measurement accuracy is fundamentally constrained by the standard quantum limit (SQL), where measurement uncertainty scales inversely with the square root of the average photon number \bar{N} within the interferometer [1–3].

Quantum mechanics provides transformative approaches for overcoming these limitations. Quantum metrology exploits distinctive quantum resources—including superposition, entanglement, and non-classical correlations—to surpass the SQL barrier and achieve ultra-high precision measurements approaching or exceeding the Heisenberg limit (HL), scaling as $1/\bar{N}$ [4–11]. This field possesses profound physical implications and demonstrates substantial potential in applications ranging from gravitational wave detection and atomic clocks to magnetometry, super-resolution imaging, and measurements of fundamental physical constants.

A principal strategy for quantum enhancement involves injecting non-classical states into interferometric devices rather than conventional coherent states. Squeezed states and entangled states generated through parametric amplification processes have proven effective for surpassing the SQL. However, preparing ideal entangled states (such as NOON states) remains challenging due to their extreme susceptibility to environmental

noise and photon loss, significantly limiting practical implementation [11–16].

Recent research has extensively explored non-Gaussian operations, particularly photon addition and subtraction, which can substantially enhance quantum states' non-classical properties and potentially improve measurement robustness. Among these, photon addition operations offer distinct advantages in quantum state preparation and in enhancing both non-classical characteristics and measurement precision [17–32]. Concurrently, interferometer architectures have been continuously refined. For instance, incorporating Kerr nonlinear media to replace conventional linear phase shifters can theoretically achieve accuracy beyond the sub-HL ($1/\bar{N}^{3/2}$), potentially reaching the super-Heisenberg limit (SHL), i.e., $1/\bar{N}^2$ [33–41].

Building upon this foundation, this work develops a quantum precision measurement scheme combining high precision with enhanced robustness. We generate two-mode squeezed coherent states (TMSCS) via four-wave mixing (FWM) and apply photon addition operations to create photon-added TMSCS (PA-TMSCS) as the interferometer input resource. Furthermore, we replace the linear phase shifter in a conventional Mach-Zehnder interferometer (MZI) with a Kerr nonlinear phase shifter, constructing a Kerr nonlinear MZI (KMZI). This study systematically analyzes the scheme's performance under both ideal conditions and in the presence of photon loss. Through examining phase sensitivity via intensity difference detection and quantum Fisher information (QFI), and comparing linear and nonlinear phase shift scenarios, we verify the synergistic advantages of photon addition operations and Kerr nonlinear effects in enhancing measurement accuracy and system resilience. This work provides valuable theoretical insights for developing practical quantum-enhanced measurement technologies.

The paper is organized as follows: Section II introduces the phase estimation model based on a KMZI with

*Corresponding author: hlyun@jxnu.edu.cn

PA-TMCS input. Section III investigates phase sensitivity of intensity difference detection for both linear ($k = 1$) and Kerr nonlinear ($k = 2$) phase shifts, including photon loss effects. Section IV examines the QFI for these cases under ideal and lossy conditions. Conclusions are presented in the final section.

II. PHASE ESTIMATION MODEL BASED ON A KMZI WITH PA-TMCS INPUT

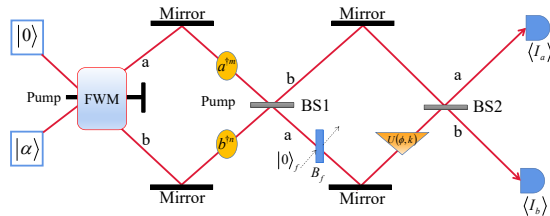


FIG. 1: Schematic diagram of phase estimation using PA-TMCS inputs in a KMZI, where photon addition operations on TMCS in both a -mode and b -mode are considered. Photon loss within the KMZI is simulated by a virtual beam splitter, and intensity difference detection is implemented at the output port.

This section presents the phase estimation model employing PA-TMCS inputs in a KMZI. As illustrated in Fig. 1, TMCS can be generated by applying an FWM process induced by a pump field to coherent states. The FWM process is equivalent to a two-mode squeezing operation described by the operator $S_2(r) = \exp[\xi^*ab - \xi a^\dagger b^\dagger]$, where $\xi = re^{i\phi_1}$, with r and ϕ_1 representing the squeezing parameter and phase, respectively. To simplify experimental procedures and avoid complicated phase-matching conditions, only the a -mode input is prepared as a coherent state $|\alpha\rangle_a$, while the b -mode input remains in the vacuum state. The coherent state satisfies $a|\alpha\rangle_a = \alpha|\alpha\rangle_a$, where $\alpha = |\alpha|e^{i\theta}$ ($|\alpha|$ and θ denote amplitude and phase, respectively). For simplicity and to satisfy phase matching conditions, we set $\theta = 0$ ($\alpha = |\alpha|$) and $\phi_1 = \pi$, which proves advantageous for enhanced phase estimation [24, 42].

To further optimize input states for improved measurement accuracy, we implement non-Gaussian photon addition operations on TMCS. The resulting PA-TMCS serves as the input state and can be expressed as

$$|\text{in}\rangle = \frac{1}{\sqrt{N_{m,n}}} a^{\dagger m} b^{\dagger n} S_2(r) |\alpha\rangle_a |0\rangle_b, \quad (1)$$

where $a^{\dagger m}$ and $b^{\dagger n}$ represent photon addition operations on the a -mode and b -mode, respectively, and $N_{m,n}$ is the normalization coefficient. To facilitate calculations, the photon addition operators in Eq. (1) can be converted to

partial derivative form:

$$|\text{in}\rangle = \frac{1}{\sqrt{N_{m,n}}} \frac{\partial^{m+n}}{\partial t_1^m \partial \tau_1^n} \exp[a^\dagger t_1] \times \exp[b^\dagger \tau_1] S_2(r) |\alpha\rangle_a |0\rangle_b |_{t_1=\tau_1=0}. \quad (2)$$

Based on this representation and quantum state normalization, the expression for $N_{m,n}$ can be derived through relevant operator transformation relations:

$$N_{m,n} = \Gamma_0 \{ \exp[((t_1 t_2 + \tau_1 \tau_2) \cosh r + (t_1 \tau_1 + t_2 \tau_2) \sinh r) \cosh r] \times \exp[((t_1 + t_2) \cosh r + (\tau_1 + \tau_2) \sinh r) \alpha] \}, \quad (3)$$

where

$$\Gamma_0 \{ \cdot \} = \frac{\partial^{2m+2n}}{\partial t_1^m \partial \tau_1^n \partial t_2^m \partial \tau_2^n} \{ \cdot \} |_{t_1=\tau_1=t_2=\tau_2=0}. \quad (4)$$

Conventional MZIs constitute linear measuring instruments comprising two 50:50 beam splitters (BS1 and BS2) and a linear phase shifter. Following Yurke *et al.* [43], using angular momentum operators in the Schwinger representation, the equivalent operators for BS1 and BS2 are $B_1 = \exp[-i\pi(a^\dagger b + ab^\dagger)/4]$ and $B_2 = \exp[i\pi(a^\dagger b + ab^\dagger)/4]$, respectively. These operators satisfy the transformation relations:

$$B_1^\dagger \begin{pmatrix} a \\ b \end{pmatrix} B_1 = \frac{\sqrt{2}}{2} \begin{pmatrix} 1 & -i \\ -i & 1 \end{pmatrix} \begin{pmatrix} a \\ b \end{pmatrix}, \quad (5)$$

and

$$B_2^\dagger \begin{pmatrix} a \\ b \end{pmatrix} B_2 = \frac{\sqrt{2}}{2} \begin{pmatrix} 1 & i \\ i & 1 \end{pmatrix} \begin{pmatrix} a \\ b \end{pmatrix}. \quad (6)$$

For our investigation, we replace the linear phase shifter in the conventional MZI with a Kerr nonlinear phase shifter to construct an improved KMZI. The phase shifter's equivalent operator is $U(\phi, k) = \exp[i\phi(a^\dagger a)^k]$, where $k = 1$ corresponds to linear phase shift and $k = 2$ to Kerr nonlinear phase shift. Here, ϕ represents the phase shift to be measured. The transformation relations for linear and Kerr nonlinear phase shifts are respectively given by:

$$U^\dagger(\phi, 1) a U(\phi, 1) = e^{i\phi} a, \quad (7)$$

and

$$U^\dagger(\phi, 2) a U(\phi, 2) = e^{i\phi} e^{i\phi(2a^\dagger a)} a. \quad (8)$$

The transformation relation for $U(\phi, 2)$ in Eq. (8) can be derived using methods from Ref. [40] based on Fock state representation, with detailed steps provided in Appendix A.

During actual measurements, photon losses inevitably occur. In our model (Fig. 1), we simulate photon losses

in the KMZI's internal *a*-mode using a virtual beam splitter placed between BS1 and the phase shifter. The corresponding transformation is:

$$B_f^\dagger \begin{pmatrix} a \\ a_f \end{pmatrix} B_f = \begin{pmatrix} \sqrt{1-l} & \sqrt{l} \\ -\sqrt{l} & \sqrt{1-l} \end{pmatrix} \begin{pmatrix} a \\ a_f \end{pmatrix}, \quad (9)$$

where a_f is the photon annihilation operator for the auxiliary mode *f* containing vacuum noise $|0\rangle_f$, while B_f and l represent the equivalent operator and reflectivity of the virtual beam splitter, respectively. The parameter l corresponds to the photon loss rate, satisfying $0 \leq l \leq 1$. Higher l values indicate increased loss, with $l = 0$ representing the lossless case and $l = 1$ corresponding to complete absorption.

Within this KMZI framework, intensity difference detection is implemented by placing photon counters at the output ports. Since intensity difference detection is relatively straightforward to implement experimentally, it finds widespread use for phase sensitivity measurements in MZIs.

III. PHASE SENSITIVITY OF INTENSITY DIFFERENCE DETECTION

The phase sensitivity for intensity difference detection can be expressed using the error propagation formula:

$$\Delta\phi = \frac{\sqrt{\langle I_D^2 \rangle - \langle I_D \rangle^2}}{\left| \frac{\partial \langle I_D \rangle}{\partial \phi} \right|}, \quad (10)$$

where $I_D = a^\dagger a - b^\dagger b$, and $\langle \cdot \rangle = \langle \text{out} | \cdot | \text{out} \rangle$ denotes the expectation value with respect to the output state. From the phase estimation model description, the output state can be expressed as:

$$|\text{out}\rangle = B_2 U(\phi, k) B_f B_1 |\text{in}\rangle |0\rangle_f. \quad (11)$$

We focus on phase sensitivity for both $k = 1$ and $k = 2$ cases. For brevity, explicit expressions for phase sensitivity are omitted here. Substituting the expectation values $\langle I_D \rangle$ and $\langle I_D^2 \rangle$ into Eq. (10) yields the phase sensitivity. The specific expressions for $\langle I_D \rangle$ and $\langle I_D^2 \rangle$ under $k = 1$ and $k = 2$ conditions are provided in Appendices B and C, respectively.

Fig. 2 illustrates the variation of phase sensitivity $\Delta\phi$ with phase shift ϕ for $k = 1$ and $k = 2$ cases, where Figs. 2(a) and 2(b) depict linear phase shift ($k = 1$), while Figs. 2(c) and 2(d) represent Kerr nonlinear phase shift ($k = 2$). According to our computational expressions and the behavior of $\Delta\phi$ in Fig. 2(a), the variation period is π . Comparing Figs. 2(a) and 2(c), curves incorporating photon addition operations show significant improvement over the black solid line ($m = n = 0$). Thus, for schemes employing PA-TMCS input states, photon addition effectively enhances phase sensitivity. Notably,

the phase sensitivity variation range in Fig. 2(c) is substantially reduced compared to Fig. 2(a) due to the Kerr nonlinear effect at $k = 2$ (hence Fig. 2(c) is not plotted over a full period), suggesting that Kerr nonlinear phase shifting can significantly improve phase sensitivity within certain phase shift ranges.

To further investigate effective photon addition schemes, we analyze phase sensitivity characteristics under narrowed plotting ranges, as shown in Figs. 2(b) and 2(d). Phase sensitivity improves with increasing photon addition order $m + n$, and near the optimal phase sensitivity point, symmetric photon addition ($m = n$) yields the best performance for a given $m + n$. This indicates that performing symmetric photon addition operations in both *a*- and *b*-modes is more conducive to enhancing measurement accuracy. Consequently, we focus on the $m = n$ scenario for photon addition operations throughout this paper.

Fig. 3 demonstrates that phase sensitivity $\Delta\phi$ improves with increasing squeezing parameter r , coherent amplitude α , and photon addition order. Additionally, comparing solid and dotted lines clearly shows that Kerr nonlinear phase shift provides improved phase sensitivity compared to linear phase shift.

In practical scenarios, photon loss constitutes an inevitable factor. We subsequently analyze its impact on phase sensitivity and compare achievable measurement precision limits. The measurement precision limit can be defined through the average photon number within the interferometer \bar{N} , expressed as:

$$\begin{aligned} \bar{N} &= \langle \text{int} | \psi | a^\dagger a + b^\dagger b | \psi \rangle_{\text{int}} \\ &= D_1(1, 0, 1, 0) + D_1(0, 1, 0, 1), \end{aligned} \quad (12)$$

where $|\psi\rangle_{\text{int}} = U(\phi, k) B_f B_1 |\text{in}\rangle |0\rangle_f$, and specific expressions for $D_1(1, 0, 1, 0)$ and $D_1(0, 1, 0, 1)$ are given in Eq. (B5) of Appendix B.

Figs. 4(a)-(c) depict linear phase shift sensitivity $\Delta\phi$ as a function of loss rate l , compared with SQL and HL. Despite photon loss, phase sensitivity can still surpass SQL, with photon addition improving system robustness. Figs. 5(a)-(c) further illustrate Kerr nonlinear phase shift sensitivity versus loss rate l . Comparison with Fig. 4 clearly shows that Kerr nonlinearity enhances phase sensitivity by an order of magnitude, enabling exceedance of the HL threshold even with loss, whereas linear phase shift only surpasses SQL within limited l ranges. However, with fixed $r = 0.9$ and $\alpha = 1$, phase sensitivity for $m = n = 0$ can exceed sub-HL, but not for $m = n = 1, 2$. This may arise from Kerr nonlinearity sensitivity to other parameters (e.g., phase shift). This situation indicates that without photon addition, phase sensitivity can exceed sub-HL within certain ranges, which is relatively favorable for Kerr nonlinearity.

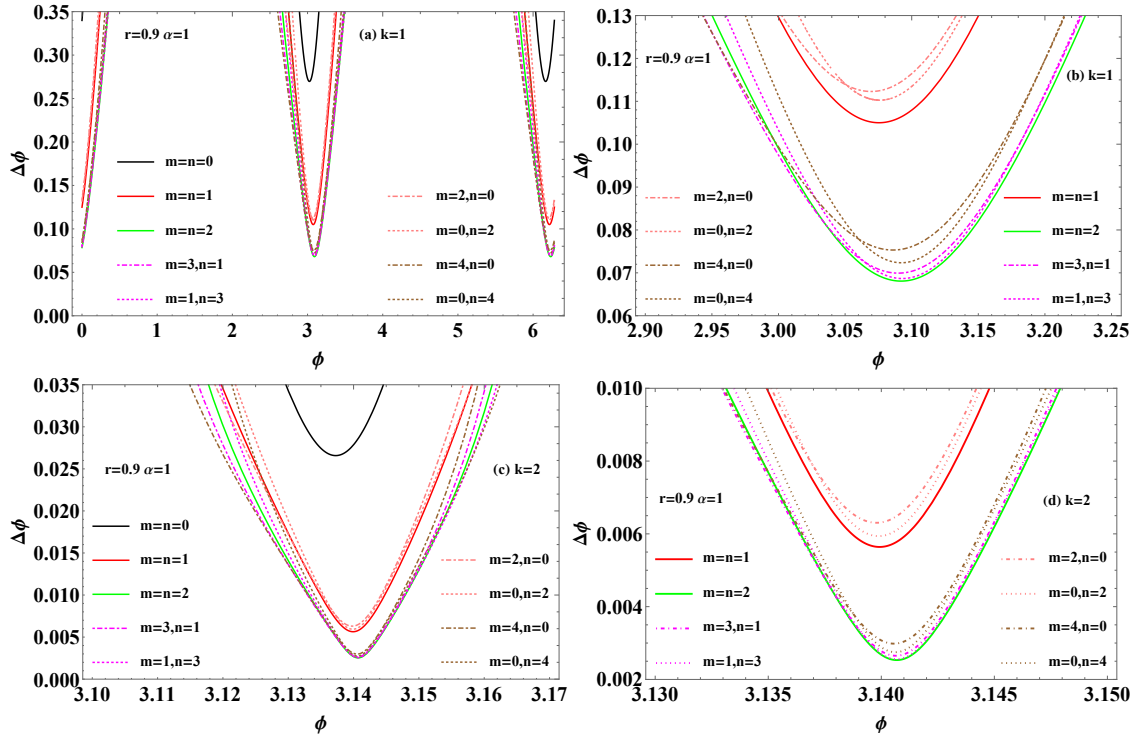


FIG. 2: Phase sensitivity $\Delta\phi$ versus phase shift ϕ for squeezing parameter $r = 0.9$ and coherent amplitude $\alpha = 1$.

IV. QUANTUM FISHER INFORMATION

A. QFI of KMZI in Ideal Case

Quantum Fisher information (QFI) quantifies the maximum information about phase shift ϕ that a quantum state can convey after passing through a phase shifter. In our scheme, employing linear and Kerr nonlinear phase shifters within the MZI leads to two corresponding QFI representations, denoted F_k ($k = 1, 2$). QFI is independent of any specific detection scheme and provides an upper bound on classical Fisher information obtainable through ϕ estimation. The optimal error bound for phase sensitivity, known as the quantum Cramér-Rao bound (QCRB), is given by [44–46]:

$$\Delta\phi_{\text{QCRB}_k} = \frac{1}{\sqrt{F_k}}. \quad (13)$$

For pure states, QFI under ideal conditions ($l = 0$) can be calculated as [47, 48]:

$$F_k = 4 \left[\langle \psi'_\phi | \psi'_\phi \rangle - |\langle \psi'_\phi | \psi_\phi \rangle|^2 \right], \quad (14)$$

where $|\psi_\phi\rangle = U(\phi, k) B_1 |\psi\rangle_{\text{in}}$ represents the quantum state before BS2 in the lossless KMZI, and $|\psi'_\phi\rangle = \partial|\psi_\phi\rangle/\partial\phi$. For both linear ($k = 1$) and Kerr nonlinear ($k = 2$) phase shifts, QFI can be further simplified as [40]:

$$F_k = 4 \langle \Delta^2 n_b^k \rangle = 4 \left[\langle (n_a^k)^2 \rangle - \langle n_a^k \rangle^2 \right], \quad (15)$$

where $\langle \cdot \rangle = \langle \Psi | \cdot | \Psi \rangle$, with $|\Psi\rangle = B_1 |\text{in}\rangle$. Here, $n_a^k = (a^\dagger a)^k$ ($k = 1, 2$). To facilitate QFI computation, the normal ordering form of n_a^w is obtained via the operator identity:

$$\begin{aligned} n_a^w &= \frac{\partial^w}{\partial x^w} \exp [x a^\dagger a] \Big|_{x=0} \\ &= \frac{\partial^w}{\partial x^w} : \exp [(e^x - 1) a^\dagger a] : \Big|_{x=0}. \end{aligned} \quad (16)$$

Since $a^\dagger a$ commutes with the phase shifter operator and losses are neglected here, utilizing the normal ordering of n_a^w allows deriving the QFI for $k = 1$ using Eq. (B5) with $l = 0$:

$$F_1 = 4 \left[D_1(2, 0, 2, 0) + D_1(1, 0, 1, 0) - D_1(1, 0, 1, 0)^2 \right], \quad (17)$$

while QFI for $k = 2$ becomes:

$$\begin{aligned} F_2 &= 4 [D_1(4, 0, 4, 0) + 6D_1(3, 0, 3, 0) \\ &\quad + 7D_1(2, 0, 2, 0) + D_1(1, 0, 1, 0) \\ &\quad - (D_1(2, 0, 2, 0) + D_1(1, 0, 1, 0))^2]. \end{aligned} \quad (18)$$

As evident from Fig. 6, increasing photon addition order significantly enhances QFI. Furthermore, comparing Figs. 6(a)-(b) with Figs. 6(c)-(d) clearly shows that the $k = 2$ case yields larger QFI values. This demonstrates that both photon addition operations and Kerr nonlinear phase shifts effectively improve QFI.

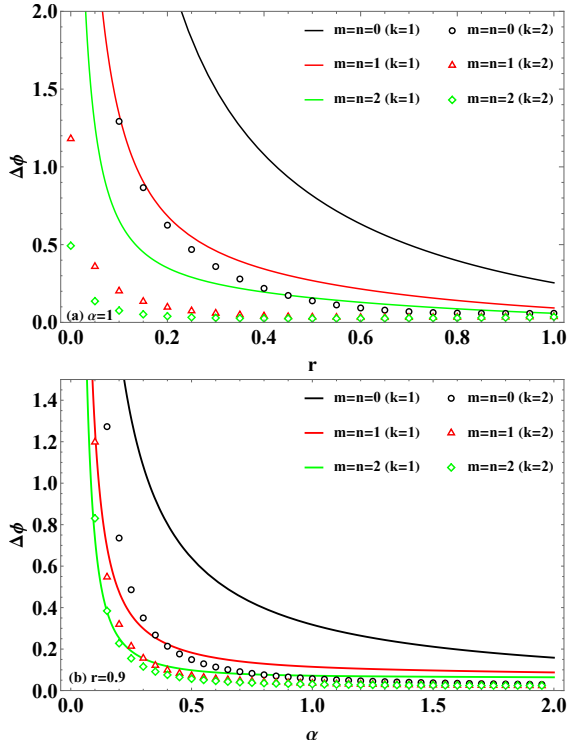


FIG. 3: For fixed phase shift $\phi = 3.12$: (a) phase sensitivity $\Delta\phi$ versus squeezing parameter r with coherent amplitude $\alpha = 1$; (b) $\Delta\phi$ versus α with $r = 0.9$.

B. Impacts of Photon Losses on QFI

1. Effects of Photon Loss on QFI in Linear Phase Shift Case ($k = 1$)

Practical measurements involve photon losses due to vacuum noise, affecting QFI. For the initial pure state $|\Psi_S\rangle$ ($|\Psi_S\rangle = B_1 |\psi\rangle_{\text{in}}$) in a probe system S with a lossy MZI, we introduce environment E orthogonal states $|j_E\rangle$ and Kraus operators $\hat{\Pi}_j(\phi)$ to characterize $|\Psi_S\rangle$ evolution through the phase shifter with photon losses. Fig. 7 illustrates the photon loss within the MZI, providing a visual representation of the model structure under investigation. Following Escher *et al.*'s methods for calculating QFI in open quantum systems [49], the quantum states $|\Psi_S\rangle$ and environment vacuum noise $|0_E\rangle$, after unitary evolution $U_{S+E}(\phi)$, can be expressed in the extended $S+E$ space:

$$|\Psi_{S+E}\rangle = U_{S+E}(\phi) |\Psi_S\rangle |0_E\rangle = \sum_{j=0}^{\infty} \hat{\Pi}_j(\phi) |\Psi_S\rangle |j_E\rangle. \quad (19)$$

Although photon losses transform $|\Psi_S\rangle$ into a mixed state, this approach allows treating $|\Psi_{S+E}\rangle$ in $S+E$ as a pure state. For the entire purified system, QFI under

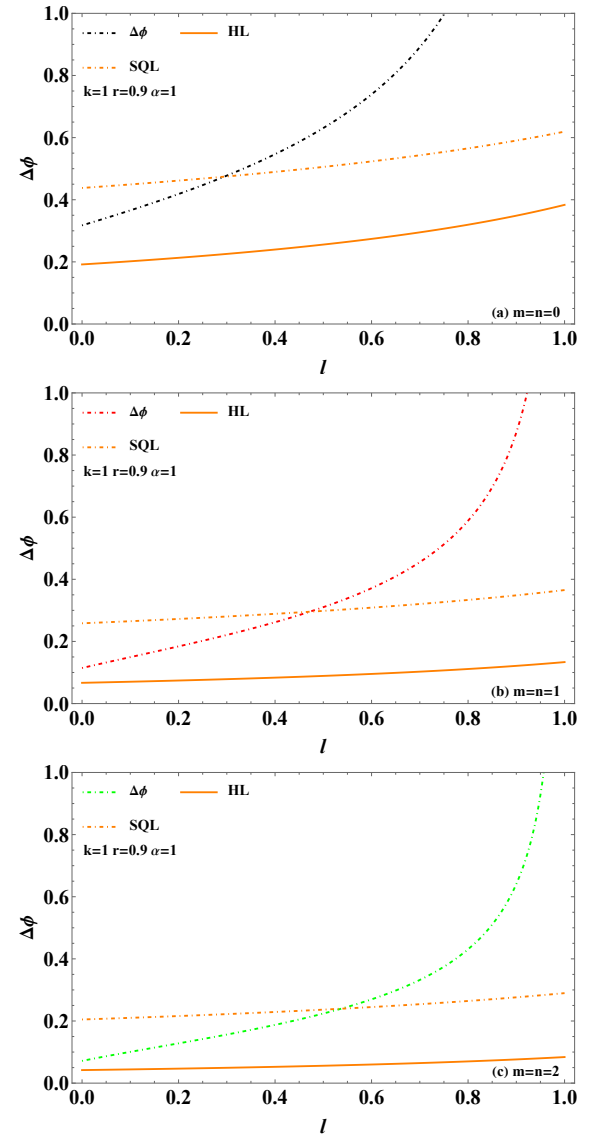


FIG. 4: Linear phase shift case: phase sensitivity $\Delta\phi$ versus loss rate l for (a) $m = n = 0$, (b) $m = n = 1$, (c) $m = n = 2$, with fixed phase shift $\phi = 3.12$, squeezing parameter $r = 0.9$, and coherent amplitude $\alpha = 1$. SQL and HL are shown for comparison.

photon losses can be expressed as:

$$F_{L_1} \leq C_Q [|\Psi_S\rangle, \hat{\Pi}_j(\phi)] = 4 \left[\langle \hat{H}_1 \rangle_S - \langle \hat{H}_2 \rangle_S \right]^2, \quad (20)$$

where the lower bound of $C_Q [|\Psi_S\rangle, \hat{\Pi}_j(\phi)]$ is shown to be the QFI for the reduced system [49], and $\hat{H}_{1,2}$ are

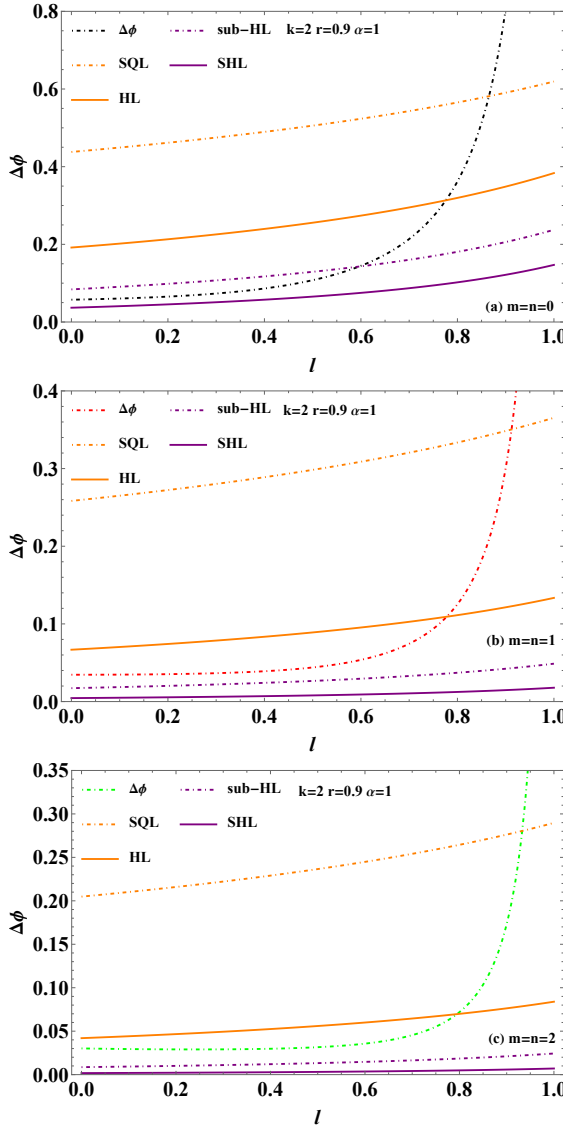


FIG. 5: Kerr nonlinear phase shift case: phase sensitivity $\Delta\phi$ versus loss rate l for (a) $m = n = 0$, (b) $m = n = 1$, (c) $m = n = 2$, with fixed phase shift $\phi = 3.12$, squeezing parameter $r = 0.9$, and coherent amplitude $\alpha = 1$. SQL, HL, sub-HL, and SHL are shown for comparison.

Hermitian operators defined as:

$$\hat{H}_1 = \sum_{j=0}^{\infty} \frac{d\hat{\Pi}_j^\dagger(\phi)}{d\phi} \frac{d\hat{\Pi}_j(\phi)}{d\phi}, \quad (21)$$

$$\hat{H}_2 = i \sum_{j=0}^{\infty} \frac{d\hat{\Pi}_j^\dagger(\phi)}{d\phi} \hat{\Pi}_j(\phi), \quad (22)$$

with $\langle \cdot \rangle_S$ denoting expectation value $\langle_S \Psi | \cdot | \Psi_S \rangle$, representing the average of $\hat{H}_{1,2}$. Thus, $F_{L_1} = C_{Q \min}$, and for

linear phase shift ($k = 1$), the Kraus operator is:

$$\hat{\Pi}_j(\phi) = \sqrt{\frac{l^j}{j!}} e^{i\phi(a^\dagger a - \gamma j)} (1-l)^{\frac{a^\dagger a}{2}} a^j, \quad (23)$$

where l is the loss rate, and $\gamma = 0$ or -1 corresponds to photon losses before or after the linear phase shifter, respectively (Fig. 7). Optimizing γ yields $C_{Q \min}$. Thus, QFI with photon losses becomes [49]:

$$F_{L_1} = \frac{4F_1(1-l)\langle n_a \rangle}{lF_1 + 4(1-l)\langle n_a \rangle}. \quad (24)$$

2. Effects of Photon Loss on QFI in Kerr Nonlinear Phase Shift Case ($k = 2$)

Extending the previous approach, we investigate QFI under photon losses for Kerr nonlinear phase shift ($k = 2$). The general Kraus operator form, incorporating Kerr nonlinear phase shift, is defined as [40]:

$$\hat{\Pi}_j(\phi) = \sqrt{\frac{l^j}{j!}} e^{i\phi[(a^\dagger a)^2 - 2\mu_1 a^\dagger a j - \mu_2 j^2]} (1-l)^{\frac{a^\dagger a}{2}} a^j, \quad (25)$$

where parameters $\mu_1 = \mu_2 = 0$ or -1 correspond to photon losses before or after the Kerr nonlinear phase shifter (Fig. 7). Referring to Eq. (20), we derive (see Appendix D for derivation):

$$\begin{aligned} F_{L_2} &\leq C_Q \left[|\Psi_S\rangle, \hat{\Pi}_j(\phi) \right] \\ &= 4 \left[K_1^2 \langle \Delta^2 n_a^2 \rangle_S - K_2 \langle n_a^3 \rangle_S \right. \\ &\quad + K_3 \langle n_a^2 \rangle_S - K_4 \langle n_a \rangle_S \\ &\quad \left. - K_5 \langle n_a^2 \rangle_S \langle n_a \rangle_S - K_6 \langle n_a \rangle_S^2 \right], \end{aligned} \quad (26)$$

where K_i ($i = 1, 2, 3, 4, 5, 6$) are detailed in Appendix D. To determine QFI F_{QL} under photon losses for Kerr nonlinear phase shift ($k = 2$), substitute optimal values $\mu_{1\text{opt}}$ and $\mu_{2\text{opt}}$ into C_Q to find $C_{Q \min}$. Specific expressions for $\mu_{1\text{opt}}$ and $\mu_{2\text{opt}}$ are provided in Appendix D. Similar to Eq. (13), $\Delta\phi_{QBL_k}$ under photon losses for $k = 1$ and $k = 2$ is derived from Eqs. (24) and (26), respectively, as $\Delta\phi_{QBL_k} = 1/\sqrt{F_{L_k}}$.

As shown in Fig. 8, despite photon loss, QCRB can still be improved through photon addition and can surpass SQL across wide loss rate l ranges, even reaching HL for small l .

Comparing Fig. 8 with Fig. 9 reveals that Kerr nonlinear phase shift ($k = 2$) significantly enhances QCRB. Despite losses, QCRB improvement through photon addition persists, with QCRB breaking through HL and sub-HL across wide l ranges, even exceeding SHL for small l . This demonstrates that although photon loss degrades QCRB, both photon addition and Kerr nonlinear phase shift can mitigate this degradation, thereby enhancing system robustness.

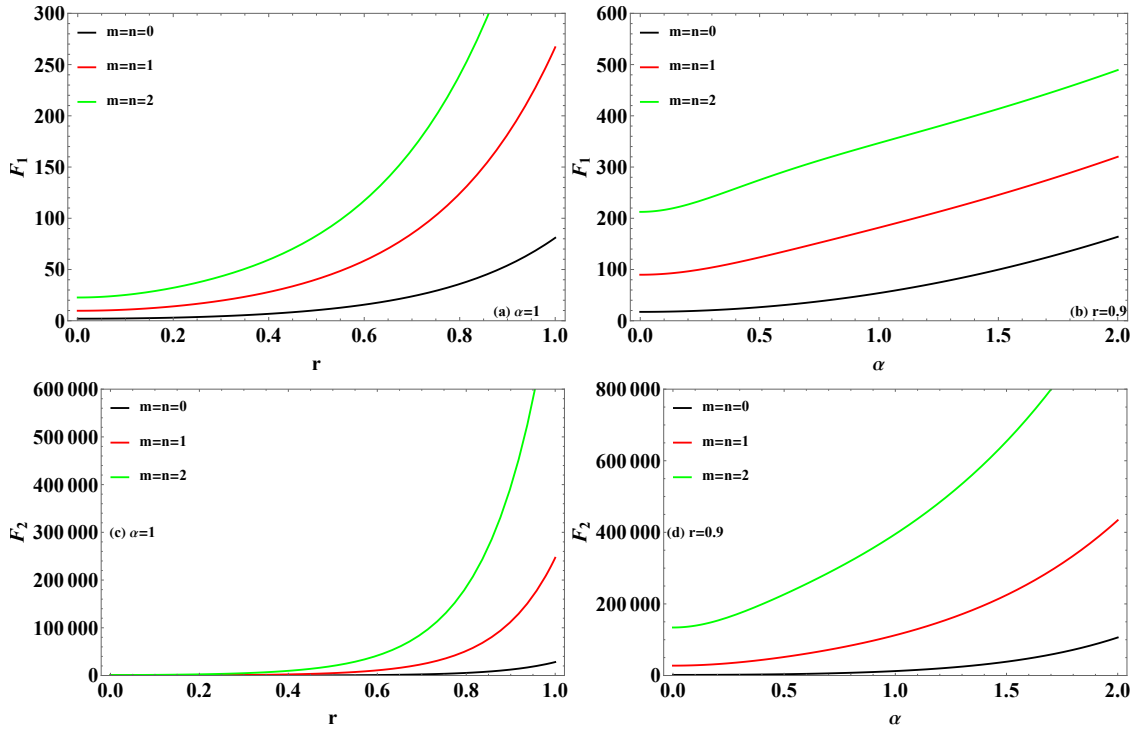


FIG. 6: For $k = 1$ case: (a) QFI F_1 versus squeezing parameter r with coherent amplitude $\alpha = 1$; (b) F_1 versus α with $r = 0.9$. For $k = 2$ case: (c) QFI F_2 versus r with $\alpha = 1$; (d) F_2 versus α with $r = 0.9$.

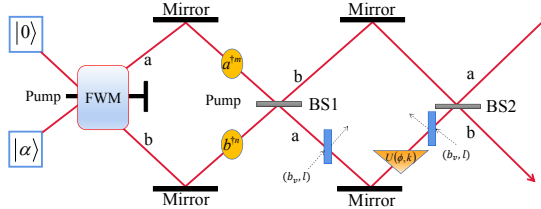


FIG. 7: Theoretical model of lossy KMZI using PA-TMCS as input. Two virtual beam splitters, positioned before and after the phase shifter, simulate photon losses. Parameter l represents beam splitter reflectivity (loss rate), while b_v denotes the vacuum operator.

V. CONCLUSION

This study demonstrates that injecting PA-TMCS into a KMZI significantly enhances phase measurement precision. By combining photon addition operations with Kerr nonlinear phase shift, we achieved measurement precision surpassing SQL and approaching sub-HL and SHL performance levels. Systematic analysis confirms that increasing photon addition order and input resource strength enhances both phase sensitivity and QFI. Crucially, the scheme maintains enhanced robustness against photon loss, providing a promising pathway toward practical quantum-enhanced metrology applications. The synergistic combination of photon addition operations and Kerr nonlinear phase shifting offers a powerful ap-

proach for achieving ultra-high precision measurements in practical quantum metrology systems.

Acknowledgments

This work is supported by the National Natural Science Foundation of China (Grants No. 12564049 and No. 12104195) and the Jiangxi Provincial Natural Science Foundation (Grants No. 20242BAB26009 and 20232BAB211033), Jiangxi Provincial Key Laboratory of Advanced Electronic Materials and Devices (Grant No. 2024SSY03011), as well as Jiangxi Civil-Military Integration Research Institute (Grant No. 2024JXRH0Y07).

APPENDIX A : DERIVATION OF TRANSFORMATION RELATION FOR KERR NONLINEAR PHASE SHIFTER OPERATOR

In the scheme proposed in this paper, the Kerr nonlinear phase shifter significantly enhances phase measurement accuracy. The associated calculations can be efficiently performed using the transformation relation of the equivalent operator of the Kerr nonlinear phase shifter, $U(\phi, 2) = e^{i\phi(a^\dagger a)^2}$, as shown in our study. Therefore, this appendix provides a detailed derivation of the transformation relation $U^\dagger(\phi, 2) b U(\phi, 2) = e^{i\phi} e^{i\phi(2a^\dagger a)} a$ in Eq. (8). Here, we assume the operator corresponding to the transformation relation of $U(\phi, 2)$

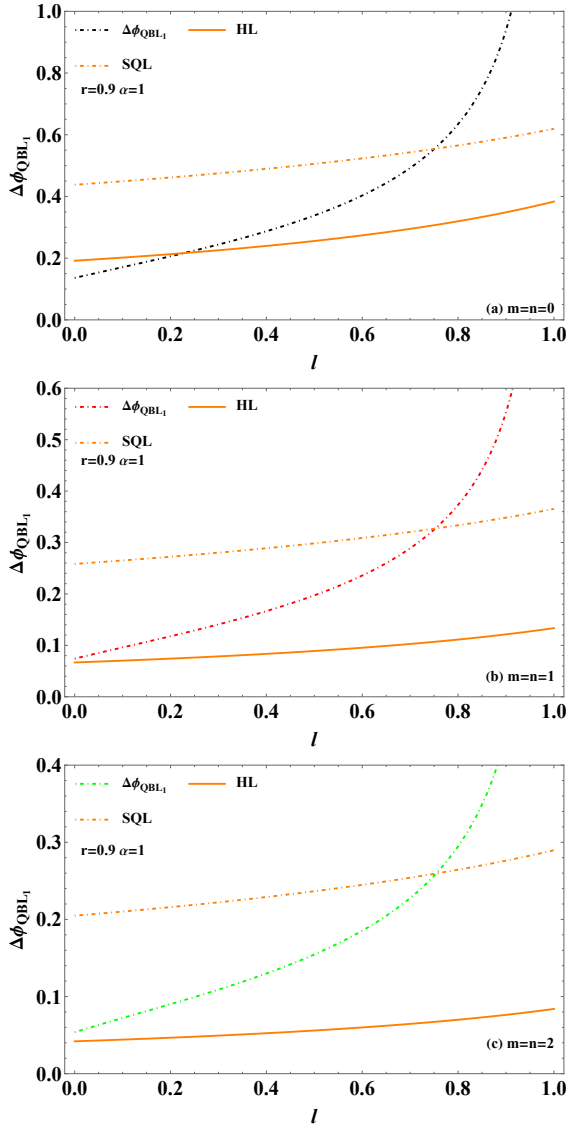


FIG. 8: For $k = 1$ case: QCRB $\Delta\phi_{QBL_1}$ versus loss rate l for (a) $m = n = 0$, (b) $m = n = 1$, (c) $m = n = 2$, with fixed squeezing parameter $r = 0.9$ and coherent amplitude $\alpha = 1$. SQL and HL are shown for comparison.

is O , i.e., $O = U^\dagger(\phi, 2) b U(\phi, 2)$. The matrix of O in the Fock state space can be represented by $O_{n,n'} = \langle n | O | n' \rangle$, and its corresponding expansion is given by

$$O = \sum_{n,n'=0}^{\infty} |n\rangle \langle n' | O_{n,n'}. \quad (\text{A1})$$

By utilizing $\langle n | b^\dagger b = \langle n | n$ and $\langle n | b = \langle n+1 | \sqrt{n+1}$, the matrix element $O_{n,n'}$ in the aforementioned equation can be further calculated as

$$O_{n,n'} = \sqrt{n+1} e^{i\phi(2n+1)} \delta_{n+1,n'}, \quad (\text{A2})$$

and by substituting it into Eq. (A1), the transformation

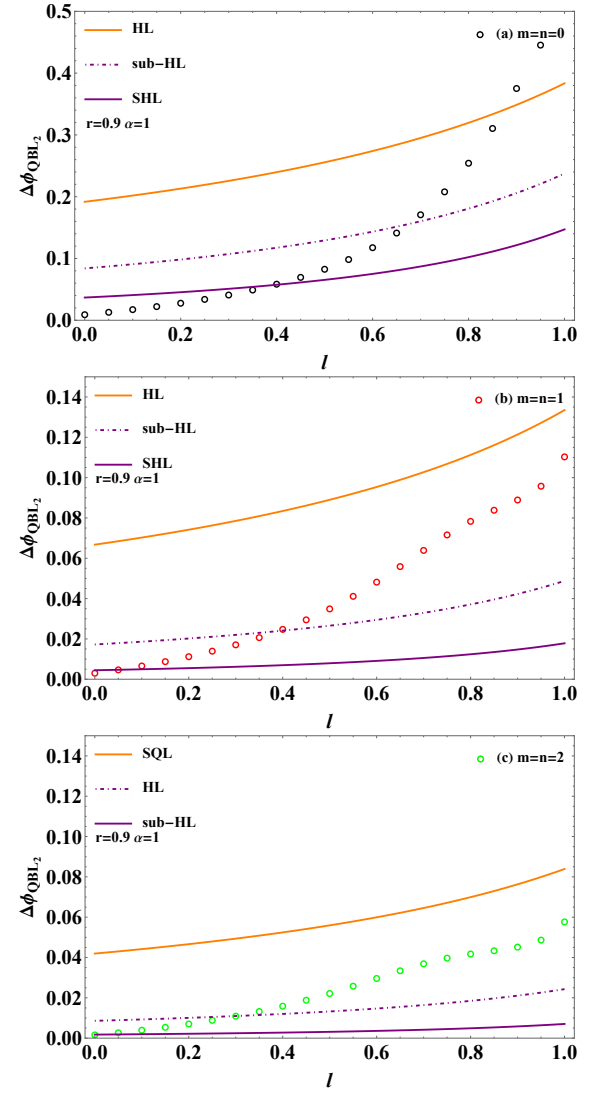


FIG. 9: For $k = 2$ case: QCRB $\Delta\phi_{QBL_2}$ versus loss rate l for (a) $m = n = 0$, (b) $m = n = 1$, (c) $m = n = 2$, with fixed squeezing parameter $r = 0.9$ and coherent amplitude $\alpha = 1$. SQL, HL, sub-HL, and SHL are shown for comparison.

relation of $U(\phi, 2)$ can be deduced as follows

$$\begin{aligned} O &= e^{i\phi} \sum_{n=0}^{\infty} |n\rangle \langle n+1 | \sqrt{n+1} e^{i2n\phi} \\ &= e^{i\phi} \sum_{n=0}^{\infty} |n\rangle \langle n | e^{i2n\phi} a = e^{i\phi} e^{i\phi(2a^\dagger a)} a, \end{aligned} \quad (\text{A3})$$

where we have used the completeness of the Fock state $\sum_{n=0}^{\infty} |n\rangle \langle n| = 1$.

APPENDIX B : THE SPECIFIC DERIVATIONS AND EXPRESSIONS FOR $\langle I_D \rangle$ AND $\langle I_D^2 \rangle$ UNDER $k = 1$ CONDITION

In order to obtain the mean values $\langle I_D \rangle$ and $\langle I_D^2 \rangle$ in Eq. (10) in a simple way, the general formula is introduced i.e.,

$$\begin{aligned} {}_f \langle 0 | \langle in | B_1^\dagger B_f^\dagger e^{-i\phi(a^\dagger a)} \\ \times (a^{\dagger m_1} b^{\dagger n_1} a^{m_2} b^{n_2}) e^{i\phi(a^\dagger a)} B_f B_1 | in \rangle | 0 \rangle_f \\ = D_1(m_1, n_1, m_2, n_2). \end{aligned} \quad (\text{B1})$$

The quantum state used in the above formula to calculate the average value is the state after passing through the phase shifter, and the output state still needs to pass through BS2. Thus using the transformation relation Eqs. (6) and (B1) one can obtain $\langle I_D \rangle$ and $\langle I_D^2 \rangle$ respectively as

$$\langle I_D \rangle = i [D_1(1, 0, 0, 1) - D_1(0, 1, 1, 0)], \quad (\text{B2})$$

and

$$\begin{aligned} \langle I_D^2 \rangle = D_1(0, 1, 0, 1) + D_1(1, 0, 1, 0) + 2D_1(1, 1, 1, 1) \\ - D_1(2, 0, 0, 2) - D_1(0, 2, 2, 0). \end{aligned} \quad (\text{B3})$$

In order to facilitate the derivation of general formula Eq. (B1), we use the following partial derivative form for representation,

$$\begin{aligned} D_1(m_1, n_1, m_2, n_2) \\ = {}_f \langle 0 | \langle in | B_1^\dagger B_f^\dagger e^{-i\phi(a^\dagger a)} \frac{\partial^{m_1+n_1+m_2+n_2}}{\partial x_1^{m_1} \partial y_1^{n_1} \partial x_2^{m_2} \partial y_2^{n_2}} \\ \exp [a^\dagger x_1 + b^\dagger y_1 + ax_2 + by_2] \Big|_{x_1=y_1=x_2=y_2=0} \\ \times e^{i\phi(a^\dagger a)} B_f B_1 | in \rangle | 0 \rangle_f. \end{aligned} \quad (\text{B4})$$

According to the transformation relationship of the corresponding operator, it can be calculated that

$$\begin{aligned} \Gamma_1 \{ \exp [\alpha(t_1 + t_2 + A_1 + A_4) \cosh r] \\ \times \exp [\alpha(\tau_1 + \tau_2 + A_2 + A_3) \sinh r] \\ \times \exp [(t_1 \sinh r + A_2 \cosh r) \tau_1 \cosh r \\ + (\tau_2 \sinh r + A_1 \cosh r) t_2 \cosh r] \\ \times \exp [(t_1 \cosh r + A_2 \sinh r) \\ \times (A_3 \sinh r + (t_2 + A_4) \cosh r) \\ \times \exp [(\tau_2 \cosh r + A_1 \sinh r) \\ \times (A_4 \sinh r + (\tau_1 + A_3) \cosh r)] \} \\ = D_1(m_1, n_1, m_2, n_2), \end{aligned} \quad (\text{B5})$$

where

$$\begin{aligned} \Gamma_1 \{ \cdot \} \\ = \frac{1}{N_{m,n}} \frac{\partial^{2m+2n+m_1+n_1+m_2+n_2}}{\partial t_1^m \partial \tau_1^n \partial t_2^m \partial \tau_2^n \partial x_1^{m_1} \partial y_1^{n_1} \partial x_2^{m_2} \partial y_2^{n_2}} \{ \cdot \} \\ |_{t_1=\tau_1=t_2=\tau_2=x_1=y_1=x_2=y_2=0}, \end{aligned} \quad (\text{B6})$$

and

$$\begin{aligned} A_1 &= \frac{\sqrt{2}}{2} \left(\sqrt{1-l} e^{-i\phi} x_1 + iy_1 \right), \\ A_2 &= \frac{\sqrt{2}}{2} \left(y_2 - i\sqrt{1-l} e^{i\phi} x_2 \right), \\ A_3 &= \frac{\sqrt{2}}{2} \left(y_1 + i\sqrt{1-l} e^{-i\phi} x_1 \right), \\ A_4 &= \frac{\sqrt{2}}{2} \left(\sqrt{1-l} e^{i\phi} x_2 - iy_2 \right). \end{aligned} \quad (\text{B7})$$

APPENDIX C : THE SPECIFIC DERIVATIONS AND EXPRESSIONS FOR $\langle I_D \rangle$ AND $\langle I_D^2 \rangle$ UNDER $k = 2$ CONDITION

With respect to operators that are partially obtained from the transformation relation of BS2, such as $a^\dagger b$, it is necessary to utilize the transformation relation of the Kerr nonlinear phase shift (Eq. (8)) and employ the IWOP technique to facilitate the calculation of the average values $\langle I_D \rangle$ and $\langle I_D^2 \rangle$. Hence, we construct the general formula

$$\begin{aligned} D_2(x) \\ = {}_f \langle 0 | \langle in | B_1^\dagger B_f^\dagger e^{-i\phi(a^\dagger a)^2} (a^\dagger b)^x e^{i\phi(a^\dagger a)^2} B_f B_1 | in \rangle | 0 \rangle_f \\ = \langle \psi | e^{-x^2 i\phi} a^{\dagger x} e^{-2x i\phi a^\dagger a} b^x | \psi \rangle \\ = \frac{\partial^x}{\partial s^x} \langle \psi | e^{-x^2 i\phi} \exp [a^\dagger b s] e^{-2x i\phi a^\dagger a} | \psi \rangle \Big|_{s=0}, \end{aligned} \quad (\text{C1})$$

where $x = 1, 2$ and for the convenience of using IWOP technology, $B_f B_1 | in \rangle | 0 \rangle_f$ is converted into a quantum state that represents a coherent state, denoted as $|\psi\rangle$. Using the following normal ordering form

$$e^{-2x i\phi a^\dagger a} =: \exp [(e^{-2x i\phi} - 1) a^\dagger a] :, \quad (\text{C2})$$

and integral formula

$$\int \frac{d^2 z}{\pi} e^{\zeta |z|^2 + \xi z + \eta z^* + fz^2 + gz^{*2}} = \frac{e^{\frac{-\zeta \xi \eta + \zeta^2 g + \eta^2 f}{\zeta^2 - 4fg}}}{\sqrt{\zeta^2 - 4fg}}, \quad (\text{C3})$$

we can compute $D_2(x)$ as

$$D_2(x) = \frac{\exp [-x^2 i\phi - \alpha^2 + M_0 + \frac{-M_1 M_2 M_3 + M_4 M_2^2 + M_5 M_3^2}{M_1^2 - 4M_4 M_5}]}{\cosh^2 r N_{m,n} \sqrt{M_1^2 - 4M_4 M_5}}, \quad (\text{C4})$$

where

$$\begin{aligned}
M_0 &= V_5(-i \tanh r (V_1 + V_2) (V_1 - V_2) V_5 \\
&\quad - i (V_1 - V_2) \tau_1 + (V_1 + V_2) V_4), \\
M_1 &= \tanh^2 r \frac{4V_1^2 + 1 + (1-l)s^2}{2} - 1, \\
M_2 &= \tau_2 + \tanh r ((V_1 + V_2) V_4 - i (V_1 - V_2) \tau_1) \\
&\quad - i \tanh^2 r (V_1 + V_2) (V_1 - V_2) V_5, \\
M_3 &= i (V_1 - V_3) V_4 + (V_1 + V_3) \tau_1 \\
&\quad + \tanh r V_5 \frac{4V_1^2 + 1 + (1-l)s^2}{2}, \\
M_4 &= i \tanh r (V_1 + V_3) (V_1 - V_3), \\
M_5 &= -i \tanh^3 r (V_1 + V_2) (V_1 - V_2), \tag{C5}
\end{aligned}$$

where

$$\begin{aligned}
V_1 &= \frac{(1-l)e^{-2xi\phi} + l}{2}, \\
V_2 &= \frac{1 + i\sqrt{1-l}s}{2}, \\
V_3 &= \frac{1 - i\sqrt{1-l}s}{2}, \\
V_4 &= t_1 + \frac{\alpha}{\cosh r}, \\
V_5 &= t_2 + \frac{\alpha}{\cosh r}. \tag{C6}
\end{aligned}$$

By further utilizing Eqs. (6), (B1) and (C1), the expressions for $\langle I_D \rangle$ and $\langle I_D^2 \rangle$ can be obtained for $k = 2$ as

$$\langle I_D \rangle = i [D_2(1) - D_2(1)^*], \tag{C7}$$

and

$$\begin{aligned}
\langle I_D^2 \rangle &= D_1(0, 1, 0, 1) + D_1(1, 0, 1, 0) \\
&\quad + 2D_1(1, 1, 1, 1) - D_2(2) - D_2(2)^*. \tag{C8}
\end{aligned}$$

APPENDIX D : C_Q FOR $k = 2$ CASE

In this appendix, we derive C_Q for the Kerr nonlinear phase shift with $k = 2$ and its specific expression to obtain the QFI F_{L_2} under photon losses condition. To compute C_Q using Eqs. (21), (22), (25) and (26) according to the method in Refs. [40] and [49], we first obtain the normal ordering form of $(1-l)^{n_b} n_a^q$ by utilizing the operator identity from Eq. (16) as follows

$$\begin{aligned}
(1-l)^{n_b} n_a^q &= \eta^{n_a} n_a^q \\
&= \frac{\partial^q}{\partial x^q} \exp [n_a \ln \eta] \exp [n_a x] \Big|_{x=0} \\
&=: \frac{\partial^q}{\partial x^q} e^{(\eta e^x - 1)a^\dagger a} \Big|_{x=0} : , \tag{D1}
\end{aligned}$$

where for simplicity, we set $\eta = 1-l$. Based on this equation and using IWOP technology, the following summation expression $S_{q,p}$ can be further calculated Based on

this equation and further utilizing the IWOP technique, the following summation can be computed for the operators associated with the Hermitian operators $H_{1,2}$ from Eqs. (21) and (22).

$$\begin{aligned}
S_{q,p} &= \sum_{j=0}^{\infty} \frac{(1-\eta)^j}{j!} j^p a^\dagger j \eta^{n_a} n_a^q a^j \\
&= \sum_{j=0}^{\infty} \frac{(1-\eta)^j}{j!} j^p : (a^\dagger a)^j \frac{\partial^q}{\partial x^q} e^{(\eta e^x - 1)a^\dagger a} \Big|_{x=0} : \\
&=: \sum_{j=0}^{\infty} \frac{[(1-\eta) a^\dagger a]^j}{j!} \frac{\partial^{q+p}}{\partial x^q \partial y^p} e^{(\eta e^x - 1)a^\dagger a + yj} \Big|_{x=y=0} : \\
&=: \frac{\partial^{q+p}}{\partial x^q \partial y^p} e^{[\eta e^x + (1-\eta) e^y - 1]a^\dagger a} \Big|_{x=y=0} : \\
&= \frac{\partial^{q+p}}{\partial x^q \partial y^p} [\eta e^x + (1-\eta) e^y]^{n_a} \Big|_{x=y=0}. \tag{D2}
\end{aligned}$$

The final step in the above equation employs the operator identity from Eq. (16) for conversion.

Similar to the calculation method for C_Q in Eq. (20), substituting the Kraus operator with $k = 2$ (Eq. (25)) into Eqs (21) and (22), and combining with Eq. (D2) and the following transformation relationships,

$$\begin{aligned}
e^{\lambda a^\dagger a} a^j e^{-\lambda a^\dagger a} &= e^{-\lambda j} a^j, \\
e^{\lambda(a^\dagger a)^2} a^j e^{-\lambda(a^\dagger a)^2} &= e^{\lambda j^2} a^j e^{-2\lambda j(a^\dagger a)}, \tag{D3}
\end{aligned}$$

we can further compute to obtain

$$\begin{aligned}
C_Q &= 4[K_1 \langle \Delta^2 n_a^2 \rangle_S - K_2 \langle n_a^3 \rangle_S + K_3 \langle n_a^2 \rangle_S \\
&\quad - K_4 \langle n_a \rangle_S - K_5 \langle n_a^2 \rangle_S \langle n_a \rangle_S - K_6 \langle n_a \rangle_S^2], \tag{D4}
\end{aligned}$$

where

$$\begin{aligned}
K_1 &= \omega_1 \eta^2 - 2\omega_2 \eta - \mu_2, \\
K_2 &= 2\eta [3\omega_1^2 \eta^3 - 3\omega_3^2 \eta^2 - \omega_4 \eta + \omega_5], \\
K_3 &= \eta [11\omega_1^2 \eta^3 - 2\omega_6^2 \eta^2 + \omega_7 \eta - 4\omega_1 \omega_2], \\
K_4 &= \eta \omega_1^2 (6\eta^3 - 12\eta^2 + 7\eta - 1), \\
K_5 &= 2(1-\eta) \eta \omega_1 K_1, \\
K_6 &= (1-\eta)^2 \eta^2 \omega_1^2, \tag{D5}
\end{aligned}$$

and

$$\begin{aligned}
\omega_1 &= 1 + 2\mu_1 - \mu_2, \\
\omega_2 &= \mu_1 - \mu_2, \\
\omega_3 &= 1 + 2(3\mu_1 - 2\mu_2) + (2\mu_1 - \mu_2)(4\mu_1 - 3\mu_2), \\
\omega_4 &= 7\mu_2 - 6\mu_1 + 24\mu_1\mu_2 - 14\mu_1^2 - 9\mu_2^2, \\
\omega_5 &= \mu_2 \omega_1 - 2\omega_2^2, \\
\omega_6 &= 9 + 40\mu_1 - 22\mu_2 + 44\mu_1^2 - 48\mu_1\mu_2 + 13\mu_2^2, \\
\omega_7 &= 7 + 40\mu_1 - 26\mu_2 + 52\mu_1^2 - 64\mu_1\mu_2 + 19\mu_2^2, \tag{D6}
\end{aligned}$$

where parameters μ_1 and μ_2 are optimizable to describe the photon losses occurring before and after the phase shifter. In particular, $\mu_1 = \mu_2 = 0$ or -1 represents photon losses occurring before or after the phase shifter, respectively, as depicted in Fig. 8. Specifically, for the case $\mu_1 = \mu_2 = -1$, $F_{L_2} \leq C_Q = 4 \langle \Delta^2 n_a^2 \rangle$, representing the ideal case of QFI. Using Eqs. (D4)-(D6), optimizing through $\partial C_Q / \partial \mu_1 = \partial C_Q / \partial \mu_2 = 0$ to find the minimum value of C_Q gives

$$\mu_{1opt} = \frac{G_2 G_5 - G_3 G_4}{G_1 G_4 - 2\eta G_2^2}, \quad (D7)$$

$$\mu_{2opt} = \frac{G_1 G_5 - 2\eta G_2 G_3}{G_1 G_4 - 2\eta G_2^2}, \quad (D8)$$

where

$$G_1 = 2 \left[- (1 - \eta) \eta \left(\langle \Delta^2 n_a^2 \rangle + 2 \langle n_a^2 \rangle \langle n_a \rangle - \langle n_a \rangle^2 \right) - (6\eta^2 - 6\eta + 1) (\langle n_a^3 \rangle + \langle n_a \rangle) + (11\eta^2 - 11\eta + 2) \langle n_a^2 \rangle \right],$$

$$G_2 = (1 - \eta)^2 \langle \Delta^2 n_a^2 \rangle + 3(1 - \eta)(2\eta - 1) \langle n_a^3 \rangle + (11\eta^2 - 13\eta + 3) \langle n_a^2 \rangle - (6\eta^2 - 6\eta + 1) \langle n_a \rangle - (1 - \eta)(2\eta - 1) \langle n_a^2 \rangle \langle n_a \rangle + \eta(1 - \eta) \langle n_a \rangle^2, \quad (D9)$$

and

$$\begin{aligned} G_3 &= \eta^2 \langle \Delta^2 n_a^2 \rangle - 3\eta(2\eta - 1) \langle n_a^3 \rangle \\ &\quad + (11\eta^2 - 9\eta + 1) \langle n_a^2 \rangle - (6\eta^2 - 6\eta + 1) \langle n_a \rangle \\ &\quad + \eta(2\eta - 1) \langle n_a^2 \rangle \langle n_a \rangle + \eta(1 - \eta) \langle n_a \rangle^2, \\ G_4 &= -(1 - \eta)^3 \langle \Delta^2 n_a^2 \rangle - 6\eta(1 - \eta)^2 \langle n_a^3 \rangle \\ &\quad - \eta(1 - \eta)(11\eta - 4) \langle n_a^2 \rangle - \eta(6\eta^2 - 6\eta + 1) \langle n_a \rangle \\ &\quad + 2\eta(1 - \eta)^2 \langle n_a^2 \rangle \langle n_a \rangle + \eta^2(1 - \eta) \langle n_a \rangle^2, \\ G_5 &= \eta \left[-\eta(1 - \eta) \left(\langle \Delta^2 n_a^2 \rangle - \langle n_a \rangle^2 \right) \right. \\ &\quad \left. - (6\eta^2 - 6\eta + 1) (\langle n_a^3 \rangle + \langle n_a \rangle) \right. \\ &\quad \left. + (11\eta^2 - 11\eta + 2) \langle n_a^2 \rangle \right. \\ &\quad \left. + (2\eta^2 - 2\eta + 1) \langle n_a^2 \rangle \langle n_a \rangle \right], \end{aligned} \quad (D10)$$

and substituting these into Eq. (D4), along with using Eq. (16) for $w = 1, 2, 3, 4$, results in $F_{L_2} = C_{Q \min}$.

[1] Ya. M. Blanter and M. Büttiker, Shot noise in mesoscopic conductors, *Phys. Rep.* **336**, 1 (2000).

[2] C. M. Caves, Quantum-mechanical noise in an interferometer, *Phys. Rev. D* **23**, 1693 (1981).

[3] N. Treps, U. Andersen, B. Buchler, P. K. Lam, A. Maître, H. A. Bachor, and C. Fabre, Surpassing the Standard Quantum Limit for Optical Imaging Using Nonclassical Multi-mode Light, *Phys. Rev. Lett.* **88**, 203601 (2002).

[4] D. Bouwmeester, J. W. Pan, K. Mattle, M. Eibl, H. Weinfurter, and A. Zeilinger, Experimental quantum teleportation, *Nature* **390**, 575 (1997).

[5] A. Acín, N. Gisin, and L. Masanes, From Bell's Theorem to Secure Quantum Key Distribution, *Phys. Rev. Lett.* **97**, 120405 (2006).

[6] B. Kraus, C. O. Ahonen, M. Möttönen, and J. L. O'Brien, Entanglement-enhanced quantum key distribution, *Phys. Rev. A* **78**, 032314 (2008).

[7] L. Y. Hu, M. Al-amri, Z. Y. Liao, and M. S. Zubairy, Continuous-variable quantum key distribution with non-Gaussian operations, *Phys. Rev. A* **102**, 012608 (2020).

[8] Z. Zhang, S. Mouradian, C. Wong, Franco N. and J. H. Shapiro, Entanglement-Enhanced Sensing in a Lossy and Noisy Environment, *Phys. Rev. Lett.* **114**, 110506 (2015).

[9] V. Giovannetti, S. Lloyd, and L. Maccone, Quantum-Enhanced Measurements: Beating the Standard Quantum Limit, *Science* **306**, 1330 (2004).

[10] H. Lee, P. Kok, and J. P. Dowling, A quantum Rosetta stone for interferometry, *J. Mod. Opt.* **49**, 2325 (2002).

[11] J. P. Dowling, Quantum optical metrology – the lowdown on high-NOON states, *Contemp. Phys.* **49**, 125 (2008).

[12] H. Cable and G. A. Durkin, Parameter Estimation with Entangled Photons Produced by Parametric Down-Conversion, *Phys. Rev. Lett.* **105**, 013603 (2010).

[13] K. Jiang, C. J. Brignac, Y. Weng, M. B. Kim, H. Lee, and J. P. Dowling, Strategies for choosing path-entangled number states for optimal robust quantum-optical metrology in the presence of loss, *Phys. Rev. A* **86**, 013826 (2012).

[14] M. W. Mitchell, J. S. Lundeen, and A. M. Steinberg, Super-resolving phase measurements with a multiphoton entangled state, *Nature* **429**, 161 (2004).

[15] I. Afek, O. Ambar, and Y. Silberberg, High-NOON States by Mixing Quantum and Classical Light, *Science* **328**, 879 (2010).

[16] J. C. F. Matthews, A. Politi, D. Bonneau, and J. L. O'Brien, Heralding Two-Photon and Four-Photon Path Entanglement on a Chip, *Phys. Rev. Lett.* **107**, 163602 (2011).

[17] A. Zavatta, S. Viciani and M. Bellini, Quantum-to-Classical Transition with Single-Photon-Added Coherent States of Light, *Science* **306**, 660 (2004).

[18] F. Jia, W. Ye, Q. Wang, L. Y. Hu, and H. Y. Fan, Comparison of nonclassical properties resulting from non-Gaussian operations, *Laser Phys. Lett.* **16**, 015201 (2019).

[19] H. Zhang, W. Ye, C. P. Wei, Y. Xia, S. K. Chang, Z. Y. Liao, and L. Y. Hu, Improved phase sensitivity in quantum optical interferometer based on multi-photon catalytic two-mode squeezed vacuum states, *Phys. Rev. A* **103**, 013705 (2021).

[20] H. Zhang, W. Ye, C. P. Wei, C. J. Liu, Z. Y. Liao, and L. Y. Hu, Improving phase estimation using number-conserving operations, *Phys. Rev. A* **103**, 052602 (2021).

[21] Y. K. Xu, S. K. Chang, C. J. Liu, L. Y. Hu, and S. Q. Liu, Phase estimation of an SU(1,1) interferometer with a co-

herent superposition squeezed vacuum in a realistic case, *Opt. Express* **30**, 38178 (2022).

[22] Y. K. Xu, T. Zhao, Q. Q. Kang, C. J. Liu, L. Y. Hu, and S. Q. Liu, Phase sensitivity of an $SU(1,1)$ interferometer in photon-loss via photon operations, *Opt. Express* **31**, 8414 (2023).

[23] L. L. Guo, Y. F. Yu, and Z. M. Zhang, Improving the phase sensitivity of an $SU(1,1)$ interferometer with photon-added squeezed vacuum light, *Opt. Express* **26**, 029099 (2018).

[24] S. Wang, X. X. Xu, Y. J. Xu, and L. J. Zhang, Quantum interferometry via a coherent state mixed with a photon-added squeezed vacuum state, *Opt. Commun.* **444**, 102-110 (2019).

[25] Y. Ouyang, S. Wang, and L. J. Zhang, Quantum optical interferometry via the photon-added two-mode squeezed vacuum states, *J. Opt. Soc. Am. B* **33**, 001373 (2016).

[26] R. Birrittella and C. C. Gerry, Quantum optical interferometry via the mixing of coherent and photon-subtracted squeezed vacuum states of light, *J. Opt. Soc. Am. B* **31**, 030586 (2014).

[27] Q. Q. Kang, Z. K. Zhao, T. Zhao, C. J. Liu, and L. Y. Hu, Phase estimation via number-conserving operation inside the $SU(1,1)$ interferometer, *Phys. Rev. A* **110**, 022432 (2024).

[28] C. Kumar, Rishabh, and S. Arora, Realistic non-Gaussian-operation scheme in parity-detection-based Mach-Zehnder quantum interferometry, *Phys. Rev. A* **105**, 052437 (2022).

[29] Y. J. Chen, J. W. Gao, J. X. Han, Z. H. Yuan, R. Q. Li, Y. Y. Jiang, and J. Song, Orbital-angular-momentum-enhanced phase estimation using non-Gaussian states with photon loss, *Phys. Rev. A* **108**, 022613 (2023).

[30] Z. K. Zhao, Q. Q. Kang, H. Zhang, T. Zhao, C. J. Liu, and L. Y. Hu, Phase estimation via coherent and photon-catalyzed squeezed vacuum states, *Opt. Express* **32**, 28267 (2024).

[31] Q. Q. Kang, Z. K. Zhao, Y. K. Xu, T. Zhao, C. J. Liu, and L. J. Hu, Phase estimation based on multi-photon subtraction operation inside the $SU(1,1)$ interferometer, *Phys. Scripta* **99**, 085111 (2024).

[32] C. Kumar, Rishabh, M. Sharma, and S. Arora, Parity-detection-based Mach-Zehnder interferometry with coherent and non-Gaussian squeezed vacuum states as inputs, *Phys. Rev. A* **108**, 012605 (2023).

[33] S. Boixo, A. Datta, S. T. Flammia, A. Shaji, E. Bagan, and C. M. Caves, Quantum Metrology: Dynamics versus Entanglement, *Phys. Rev. A* **77**, 012317 (2008).

[34] J. Joo, K. Park, H. Jeong, W. J. Munro, K. Nemoto, and T. P. Spiller, Quantum metrology for nonlinear phase shifts with entangled coherent states, *Phys. Rev. A* **86**, 043828 (2012).

[35] C. P. Wei and Z. M. Zhang, Improving the phase sensitivity of a Mach-Zehnder interferometer via a nonlinear phase shifter, *J. Mod. Opt.* **64**, 743 (2017).

[36] J. D. Zhang and S. Wang, Nonlinear phase estimation based on nonlinear interferometers with coherent and squeezed vacuum light, *Phys. Lett. A*, **502**, 129400 (2024).

[37] G. F. Jiao, K. Y. Zhang, L. Q. Chen, W. P. Zhang, and C. H. Yuan, Nonlinear phase estimation enhanced by an actively correlated Mach-Zehnder interferometer, *Phys. Rev. A* **102**, 033520 (2020).

[38] G. F. Jiao, Q. Wang, Z. F. Yu, L. Q. Chen, W. P. Zhang, and C. H. Yuan, Effects of losses on the sensitivity of an actively correlated Mach-Zehnder interferometer, *Phys. Rev. A* **104**, 013725 (2021).

[39] S. K. Chang, C. P. Wei, H. Zhang, Y. Xia, W. Ye, and L. Y. Hu, Enhanced phase sensitivity with a nonconventional interferometer and nonlinear phase shifter, *Phys. Lett. A*, **384**, 126755 (2020).

[40] S. K. Chang, W. Ye, H. Zhang, L. Y. Hu, J. H. Huang, and S. Q. Liu, Improvement of phase sensitivity in an $SU(1,1)$ interferometer via a phase shift induced by a Kerr medium, *Phys. Rev. A* **105**, 033704 (2022).

[41] J. D. Zhang, Z. J. Zhang, L. Z. Cen, J. Y. Hu, and Y. Zhao, Nonlinear phase estimation: Parity measurement approaches the quantum Cramér-Rao bound for coherent states, *Phys. Rev. A* **99**, 022106 (2019).

[42] K. P. Seshadreesan, P. M. Anisimov, H. Lee, and J. P. Dowling, Parity detection achieves the Heisenberg limit in interferometry with coherent mixed with squeezed vacuum light, *New J. Phys.* **13**, 083026 (2011).

[43] B. Yurke, S. L. McCall, and J. R. Klauder, $SU(2)$ and $SU(1,1)$ interferometers, *Phys. Rev. A* **33**, 4033 (1986).

[44] S. L. Braunstein and C. M. Caves, Statistical distance and the geometry of quantum states, *Phys. Rev. Lett.* **72**, 3439 (2013).

[45] S. L. Luo, Wigner-Yanase Skew Information and Uncertainty Relations, *Phys. Rev. Lett.* **91**, 180403 (2003).

[46] Z. Y. Ou, Complementarity and Fundamental Limit in Precision Phase Measurement, *Phys. Rev. Lett.* **77**, 2352 (1996).

[47] C. W. Helstrom, *Quantum detection and estimation theory* (Academic, New York, 1976).

[48] J. Liu, X. X. Jing, W. Zhong, and X. G. Wang, Quantum Fisher information for density matrices with arbitrary ranks, *Commun. Theor. Phys.* **61**, 45 (2014).

[49] B. M. Escher, R. L. de Matos Filho, and L. Davidovich, General framework for estimating the ultimate precision limit in noisy quantum-enhanced metrology, *Nat. Phys.* **7**, 406 (2011).